FABRICATION AND OPTIMIZATION OF SILICON SOLAR CELL CHARACTERISTICS BY USING POROUS SILICON LAYERS ON THE FRONT AND BACK SIDES

Hager A. Nawar [1], Gamal M. Youssef[2], Mahmoud M. El-Nhass[3] and Mohamed GH. El-Malky[1]

[1] Basic Science Department, Institute of Environmental Studies & Research, Ain Shams University

[2]Physics Department, Faculty of science, Ain Shams University

[3] Physics Department, Faculty of Education, Ain Shams University

ABSTTRACT

Porous silicon layer (PSL) has emerged in potential solar cell applications because of its high surface area to volume ratio, convenient surface chemistry and large energy band gap ≈1.9 ev. PSL has been prepared from n^+p/Si junction using electrochemical etching (ECE) with three different current densities 25, 50 and 75 mA/cm^2 on the front and back side of the junction. The influence of varying current density on morphological, optical, chemical and electrical properties of PS has been inspected. SEM micrographs showed that the surface porosity of 90% on the front side, in contrast the etched back surface seemed in harmonic shape with identical pore size and porosity of 98%. The PL spectrum peak ranged from 640 to 670 nm. PSL formed on both sides has the lowest reflectivity at current density of 50 mA/cm^2. The obtained

FTIR spectra of the samples with a relatively high PL intensity exhibit a developed broad transmission bands in the range of 600 to 4000cm^{-1} Solar cell conversion efficiency of PSL formed on both sides is increased to 17% compared to other workers. Solar cell based on PSL formed on both sides provides stability and it is be recommended for industry manufacturing.

KEYWORDS: Porous silicon, Solar cell, Photoluminescence and Reflectance.

INTRODUCTION

Silicon (Si) is a suitable photovoltaic (PV) material due to its measured Energy band gap (E_g) =1.12 eV and availability, especially when compared to PV substrate such as titanium dioxide (TiO_2) of E_g = 3.20 eV and cadmium selenide (CdSe) of E_g =1.94 eV and cadmium sulphide (CdS)of E_g = 2.42 eV, that all have higher bandgaps **(Sun et al., 2014)**.

PSL was discovered coincidentally in 1956 by Uhlir while investigating the electrolytic etching of Si in hydrofluoric (HF) acid solutions. Since that, PSL has been harnessed for applications such as optoelectronics **(Bisi *et al*., 2000)**, solar cells **(Dzhafarov, 2013)**, batteries **(Fang *et al*., 2013)**, and biomedical applications **(Anglin *et al*., 2006)**. PSL is considered as a nano arranged form of silicon with a large surface volume ratio, that is fabricated through ECE technique **(Sailor, 2014)**. the Photocurrent efficiency with n-type and p-type PSL (100) wafers of different crystal orientations had shown an increase in solar power when compared to planar silicon without PSL **Salman**

***et al* (2012)**. However, the porosity of n-type PSL (100) was, much higher than for PSL p-type silicon (100). This research implied that Si solar cells that were modified with a PSL structure could considerably improve the maximum solar power. In contrast, the conversion efficiency of PSL formed on both sides increased in compared with one side etched sample **Ramzy *et al* (2011)**. Surface texturing of Si also improves the antireflective properties, which reinforcing light trapping and conversion efficiency when compared to conventional Si solar cells, the importance of PSL in Si solar cells fabrication were summarized with **(Dzhafarov, 2013)**.

In this research, we recently investigated the effect of PSL based on front, back and both sides of n^+p/Si junction on the electrical properties of Si solar cell and to investigate the morphological structures, optical properties and chemical composition of the prepared samples.

EXPRIMENTAL DETAILS

CZ -Si substrate of p type (100) with resistivity of 5.0 Ω. cm thickness ≈ 450 µm have been textured **(Schneider *et al*., 2014)** and undertaken a typical cleaning before the diffusion of phosphorus emitter ($POCl_3$), it has been used to longwinded textured substrates underneath optimum condition in order to generate an n^+p/Si junction on the front side of the material, the thickness of n layer was ≈ 1 µm. The substrate of type n^+p/Si were cut in to small pieces of size 1.5x2.0 cm^2 that was well-suited with the width of substrate holder by

using a harden cutter tool. Thin homogenous PSL of different thicknesses were formed on the front n and back p-side surface of the material using ECE process. Before starting ECE, the samples were heated in Isopropyl Alcohol (IPA) at 75 C° for 30 min. Many studies reported that adding (IPA) increases the wettability of the silicon surface and then removes the observing hydrogen bubbles sticking on the surface **(OU *et al*., 2011; Youssef et al., 2015b)**, after that the small pieces of samples were immersed in deionized water (DI) water for 5.0 min and dried under the stream of nitrogen gas.

The ECE process was performed to produce three groups of samples by using a 1:3 mixture of 40 % HF: 95 % ethanol (volume ratio) as an electrolyte and variation of current density of 25, 50 and 75 mA/cm² for group I, group II and 50 mA/cm² for group III under a fixed etching time of 25 min. Group I consists of 3 samples of PSL (Sn_1, Sn_2 and Sn_3) formed on the front n-side [PS/n^+p/Si], group II consists of 3 samples of PSL (Sp_1, Sp_2 and Sp_3) formed on the back p-side [PS/pn^+/Si] and group III consists of 2 samples of PSL (Sn_4 and Sp_4) formed on the both sides [PS/n^+p/Si/PS] and [PS/p n^+/Si/ PS]respectively. the formation of PSL by ECE process was done without any illumination **(Yerokhov *et al*., 2000; Youssef *et al*., 2015a).**

Ethanol is usually added to make the removal of H_2 bubbles simpler, these bubbles can easily affect the surface since the liquid surface tension is decreased. Moreover, the mixing of ethanol in electrolyte helps to improve the

uniformity of the PSL **(Dubey and. Gautam, 2009)**. To form a good ohmic contact, Al electrode was placed in back contact with samples and acts as anode. The platinum (Pt) counter acts as cathode as shown in **Fig. 1**.

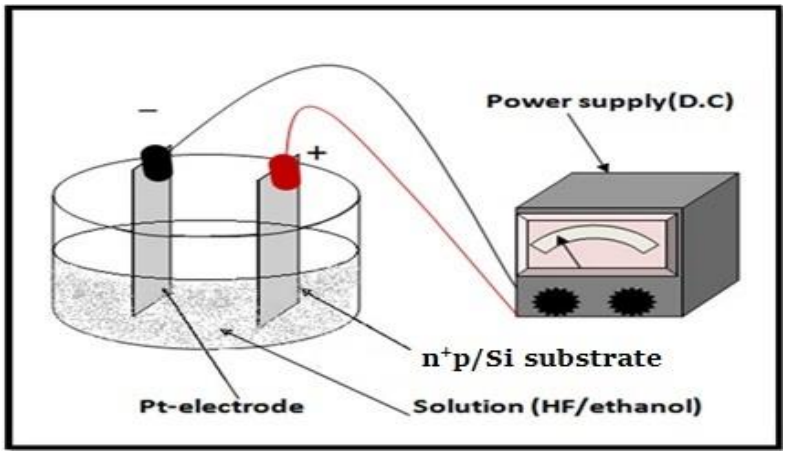

Figure 1: The electrochemical etching system (schematic diagram).

The anodization process was carried out with the distance between the sample to the Pt counter electrode fixed at ≈ 1.0 cm. After the anodization, the PSL were rinsed first with acetone for 2.0 min, then with 95% Ethanol for 2.0 min, and finally with deionized water. the samples were dried with a stream of nitrogen gas at low pressure to protect PSL surface formed from cracking.

To formulate solar cell: after PSL formed on the surface of both front n and back p-side of samples. Aluminum (Al) evaporation was used for back surface contact and gold (Au) for front metallization. The evaporation process

was carried out using high vacuum coating unit (Edward E306A England), the samples-coated electrodes were annealed at 450c^{o} in argon atmosphere. The construction of PSL solar cell be made up of metal mask of grid pattern with

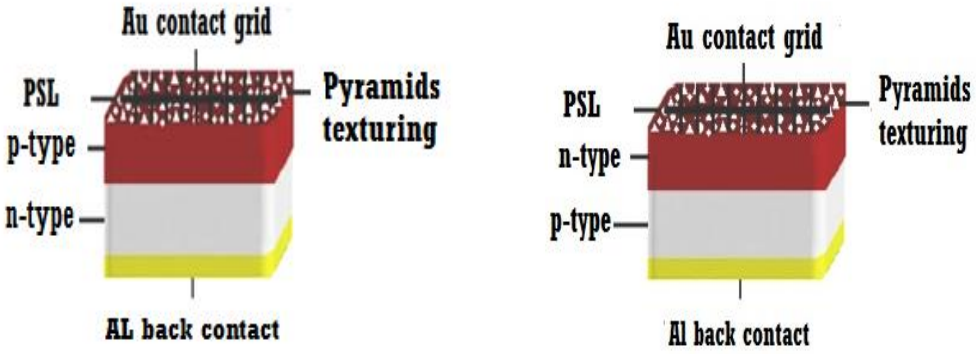

finer width of 0.05 cm and finger spacing of 0.1 cm.

(a) **(b)**

Figure 2. Solar cells based on PSL and pyramids texturing samples for (a): front n-side and (b): back p-side.

Morphological properties of the PSL formed on the front n-side and back p-side are characterized by using high resolution scanning electron microscopy (SEM) inspect S. The photoluminescence (PL) measurement were carried out using (RF-5301 Spectrofluorophotometer, Shimadzu) by using 150W Xenon excitation lamp with wavelengths are in range of 200-999 nm. spectrophotometer (UV VIS-NIR 3600 Spectrometer, Shimadzu) used to record surface reflectivity of PSL. Fourier transform infrared (FTIR) spectrometer

used for the measurement of chemical composition of PSL samples is a (Nicolet 6900 FTIR, thermoscientific, class1). Finally, electrical (J-V) characteristics of samples have been measured after fabrication of the solar cell device by using keithely 2400 source meter.

EXPERIMENTAL RESULTS AND DISSCUSSION

1.Surface morphology:

1.1. Group I samples:

Figure 3-a shows SEM of the front n-surface without PSL formation, the shape of the front n-surface is presented in pyramidal form. By starting ECE process and applying current density of 25 mA/cm² **Fig. 3-b**, A discrete pores with small size are shaped, the whole surface is blocked with spiderwebbed (sample Sn_1). When current density is increased to 50 mA/cm² (sample $Sn_{2)}$ **Fig. 3-c,** the obtained pores become more homogeneous and disciplined in size and the whole surface is entangled. By implementation of current density of 75 mA/cm² (sample $Sn_{3)}$, an important notice that the number of pores are decreased, and the surface is intermittent with dendritic wall pattern **Fig. 3-d.** the average pore diameter and thickness of samples are listed in **Table 1**.

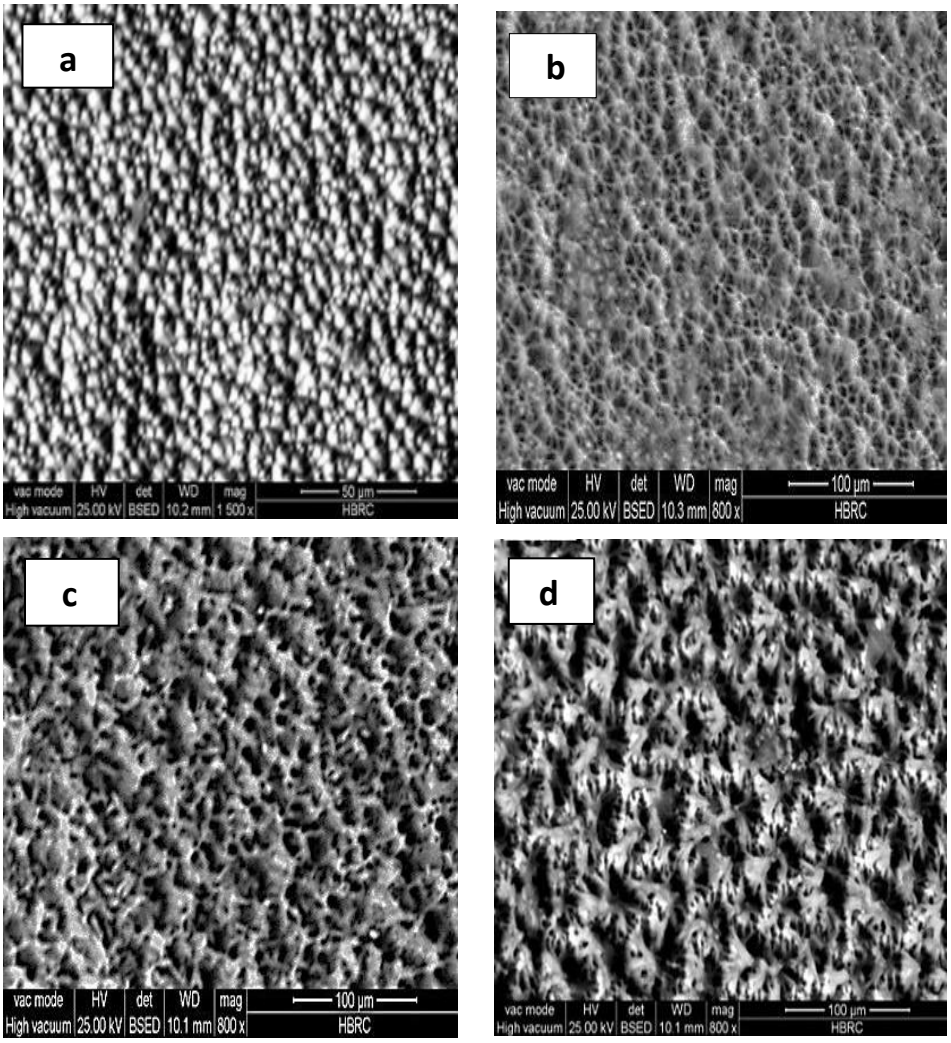

Figure 3. SEM of: (a) front $n^{+}p/Si$ without PSL, (b), (c) and (d) for PSL samples Sn_1, Sn_2 and Sn_3 prepared at 25, 50 & 75 mA/cm² for fixed time of 25 min and electrolyte concentration (1:3).

1.2. Group II samples:

Figure 5-a represents SEM of the back p-surface without PSL, the shape is also organized in pyramidal form, but the size of pyramids is seemed to be smaller than that of the front n-surface **(Fig.3-a)**. By applying current density of 25 mA/cm² (sample Sp_1), many disconnected holes are presents **Fig.4-b** however, the pore is greater in number and the surface seems to be more etched in compare with that appears in sample Sn_1. When current density is increased to 50 mA/cm² **Fig. 4-c,** the surface seems in Harmonic shape with identical pore size and encashments in addition that, the obtained pores are larger in size than in sample Sp_1 and the pores appear totally couple with each other in compare with the pore formed on the front n-surface (sample Sn_2) that has discrete pores with smooth walls, in addition to short branches pores. **(salman *et al*., 2012, Youssef *et al*., 2015b)**. With operation of current density of 75 mA/cm² **Fig. 4-d**, the surface is distributed in branched wedges (sample Sp_3), and the pore size is shrunken in compare with pore shaped on sample Sn_3 **(Kulathuraan *et al*., 2016).** the average pore diameter and thickness of samples are listed in **Table 1**.

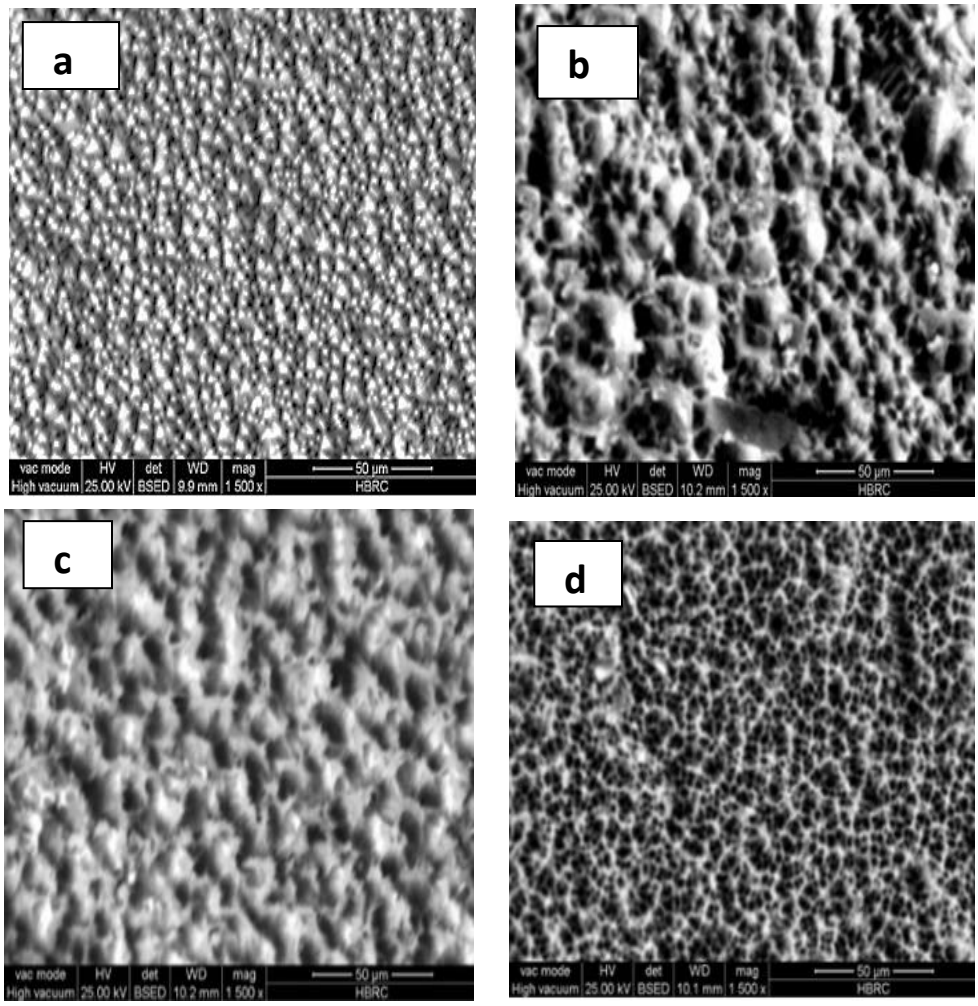

Figure 4. SEM for: (a): $n^{+}p/Si$ without PSL, (b), (c) and (d) for PSL samples Sp_1, Sp_2 and Sp_3 prepared at 25, 50 & 75 mA/cm² for fixed time of 25 min and electrolyte concentration (1:3).

The term porosity can be defined as a function of geometrical parameters is given in **Eq. 1** (**Salcedo *et al*., 1999, Kulathuraan *et al*., 2016**),

$$P = \left(\frac{\pi}{2} * 1.932\right) \left(\frac{1}{1+\frac{m}{d}}\right)^2 \ldots\ldots\ldots\ldots\ldots\ldots (1)$$

Where d is the average pore size and m is the distance between pores. Using the above equation, the calculated porosity values are given in **Table 1**.

Table 1. Average pore diameter, measured thickness & Porosity for PSL prepared on the front n–side (samples Sn_1, Sn_2 and Sn_3) and the back p–side (Sp_1, Sp_2 and Sp_3).

Sample	Average pore diameter (µm)	Measured thickness (µm)	Porosity %	Sample	Average pore diameter (µm)	Measured thickness (µm)	Porosity %
Sn_1	4.0	45.2	73.6	**Sp_1**	3.6	13.0	80
Sn_2	6.4	67.2	90.0	**Sp_2**	6.1	33.5	98
Sn_3	5.6	50.0	79.0	**Sp_3**	4.5	16.0	87

So, we can conclude that the samples Sn_2 and Sp_2 at current density of 50 mA/cm² exhibit the most uniform homogeneous PSL surface and quantum wire structure of thin string pillar silicon walls, it may be expected to exhibit the quantum confinement effects (QCE) owing to the aggregates of nano crystallite silicon in the etched layer. **(Dian *et al*., 2004).**

2-Photoluminescence spectra (PL):

2.1. GroupI samples:

Figure 5-a express PL spectra of PSL formed on the front n-side Sn_1, Sn_2 and Sn3 for different etching current densities with the excitation wavelength at λ= 325 nm. The emitted band is detected around 685 and the calculated E_g using the PL spectra giving in **Eq. 2** is found in the range of 1.91 eV.

$$E_g = \frac{1240}{\lambda} \quad \text{..... (2)}$$

The increasing value in E_g indicates that, blue shift maximum and the particles are confined to the lower dimension which directed to high efficiency according to the quantum confinement effects **(Omar, 2009; Ramizy *et al.*, 2011, Salman, 2012; Kulathuraan *et al.*, 2016, Youssef, 2016)**. This is as result of increasing the total volume of the pores and relative to the number of released photons on the PSL surface (SEM studies), While the PL intensity emission band drop for sample Sn_3. A possible reason might be formation of dendritic pore pattern, broadening of the pore walls and decrease numbers of pores on the PSL surface and thus decreases the porosity (SEM results) which prevents good light absorption.

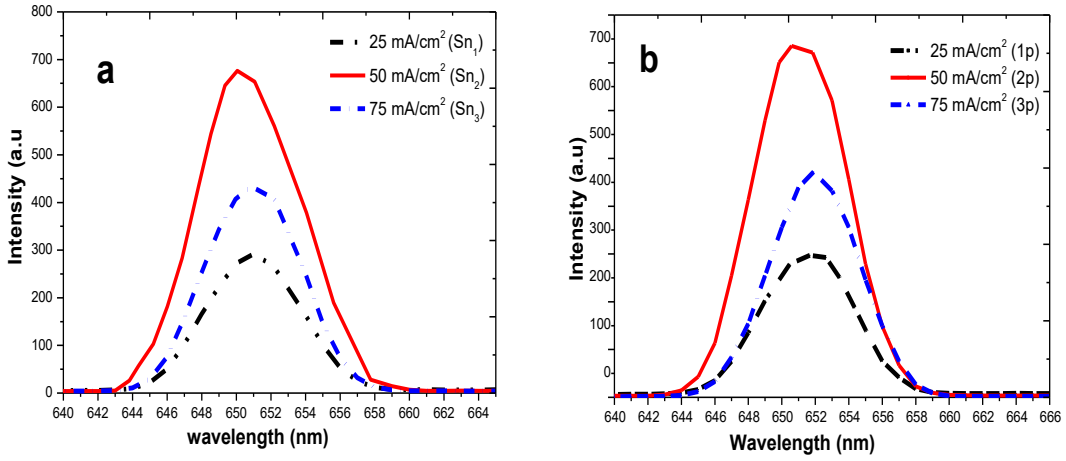

Figure 5. Photoluminescence of PSL samples prepared on (a): the front n-side (Sn_1, Sn_2 and Sn_3) and (b): back p-side (Sp_1, Sp_2 and Sp_3)

2.2. Group II samples:

Figure 5-b describe the PL spectra of PSL formed on the back p-side Sp_1, Sp_2 and Sp_3. The result is similar to that obtained in group I samples, The maximum peak intensity accomplish to 675 (a.u) for sample SP_2 and the computed E_g using **Eq. 2** is about 1.905 (ev) while, the intensity peak for sample Sp_3 is decreased to 430 (a.u) as a result of the discount in average pore size and layer thickness, and thus decreasing its porosity this come to an agreement with other reporters **(Rajabi *et al*., 2009; Kulathuraan *et al*., 2016)**. The recorded PL intensities (broadening and height) and hence obtained Eg_s of PSL formed on front n-side are higher than that formed on the back p-side

because of the effect of the growth of its average pore size and layer thickness see

Sample	ג (nm)	Intensity (a.u)	FWHM (nm)	E_g (e.v)
Group I				
Sn_1	651.4	280	6.0	1.903
Sn_2	649.8	685	8.0	1.910
Sn_3	651.0	430	7.5	1.904
Group II				
Sp_1	651.7	240	6.0	1.902
Sp_2	650.6	675	7.5	1.905
Sp_3	651.9	420	7.0	1.903

Table 2.

Table 2. intensity, FWHM and calculated Eg for: PSL samples prepared on front n–side (Sn_1, Sn_2 and Sn_3) and back p–side (Sp_1, Sp_2 and Sp_3).

3. Reflectance measurements:

3.1. Group I samples:

Figure 6-a illustrates the reflection spectra of PSL samples formed on front n side. The reflectance decreases from 12.8% to 9.6% and then increasing

again to 10.5% for samples Sp_1, Sp_2 and Sp_3 respectively compared with that without PSL (R=35%). The lowest effective light reflection is obtained from sample Sn_2 that consisted of meso-pores compared with reflectivity's of the other samples.

The maximum reduction in light reflection ranged from 300 to 700 nm, due to the increasing in the roughness expected to increase the light scattering in PSL, then reduce the reflectivity. Using PSL as antireflection coating (ARC) layer in the solar cells designs is a very important, it lead to the increase in light absorption in the visible region of the solar spectrum that is predictable to increase the efficiency of solar cells.

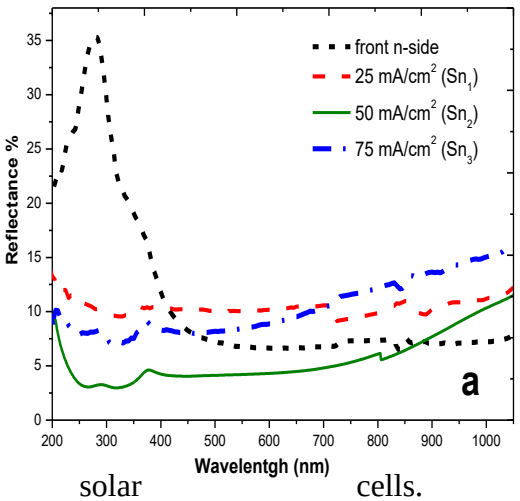

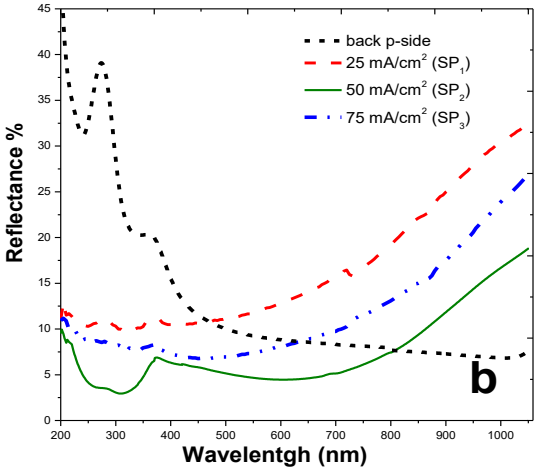

Figure 6. Reflectance of PSL samples prepared on (a): the front n-side (Sn_1, Sn_2 and Sn_3) and (b): back p-side (Sp_1, Sp_2 and Sp_3) corresponding to front n and back p-side without PSL layer.

3.2. Group II samples:

The reflectance curve that obtained in PSL samples formed on back p-side are presented in **Fig. 6-b**. The reflectance decreases from 12.5% to 10% and then increasing again to 11.2 % for PSL samples: Sp_1, Sp_2, Sp_3 respectively compared with that of back p-side sample without PSL (R=39%). this agrees with the previous results obtained from PL measurements. In general comparison the reflectivity curves measured for PSL samples formed on front n-side PSL are higher than that measured for PSL samples formed on back p-side. this can be due to the increasing in pore size and layer thickness leads to increasing in light absorbing and decreasing its surface reflectivity. this agree with pervious author's **(Ramizy *et al*., 2011; salman *et al*., 2012, Youssef *et al*., 2016)**.

As in similar, the sample Sp_2 give the most lower surface reflectivity response comparing to other sample data recorded (Sp_1 and Sp_3). these results lead to a conclusion that both samples Sn_2 and Sp_2 give the best optimum reflectivity data obtained and hence are most profitable to be used in manufacturing the solar cells and is predictable to increase light absorption in the visible region of the solar spectrum so that increasing the solar cells efficiency.

3.3. Optical E_g calculation:

E_g values for PSL formed on front n and back p-side are calculated from reflectivity curves by using Ku-Munk Equation (**Kubelka, 1931; Kubelka, 1946; Tauc *et al*., 1966)** and listed in **Table 3,**

$$\mathbf{F(R)}h\upsilon = \mathbf{A}\left(h\upsilon - \mathbf{E_g}\right)^{\mathbf{n}} \text{.....(3)}$$

Where F(R) is proportional to the absorption coefficient (α). And **F(R)=** $\frac{(1-R)^2}{2R}$ **(Otsuka, 2004)** and A is the edge width parameter representing the film quality, $h\upsilon$ is the incident photon energy, $\mathbf{E_g}$ is optical gap and n is constant determines the type of transition, n= 1/2, for the direct allowed transition and 2 for indirect allowed transition.

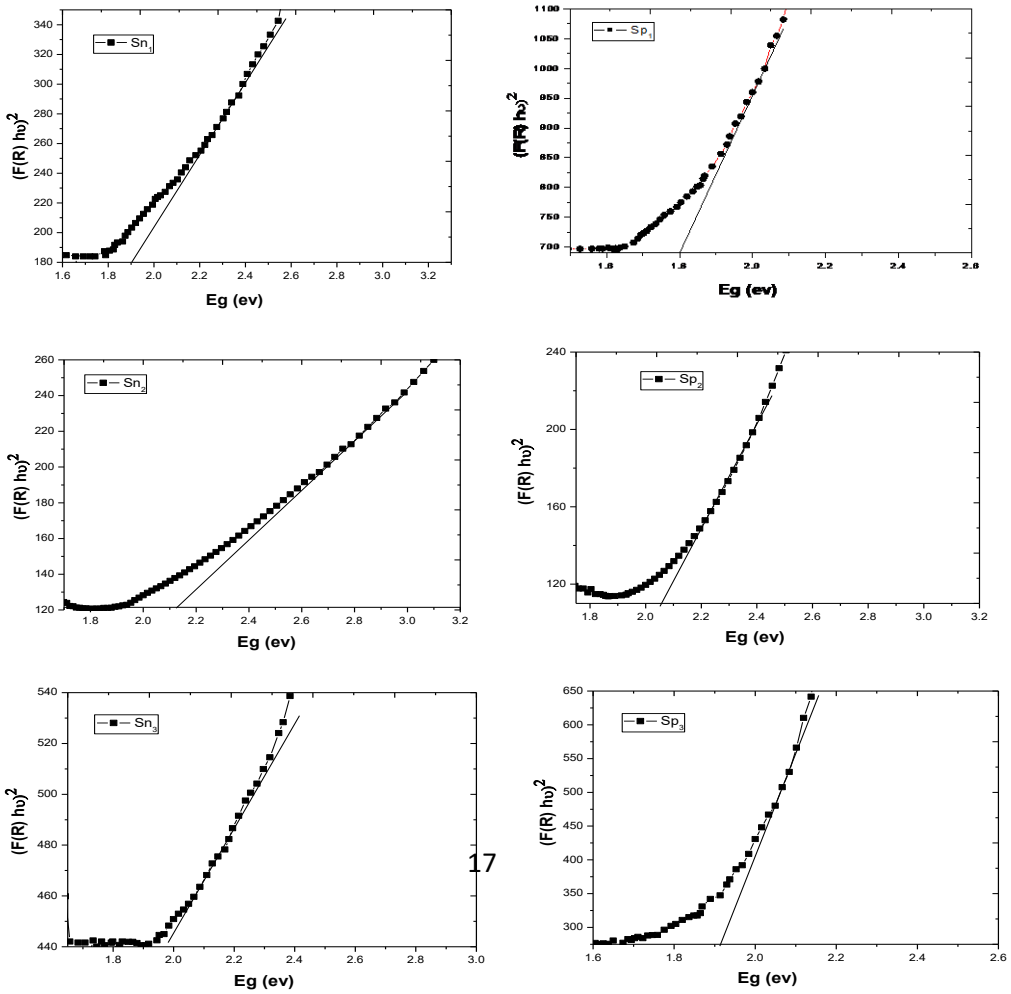

(a) **(b)**

Figure 7. Different plots of $(F(R)\ h\nu)^2$ versus hν for PSL samples prepared on (a): the front n-side (Sn_1, Sn_2 and Sn_3) and (b): back p-side (Sp_1, Sp_2 and Sp_3).

Table 3. give comparison between the calculated band gap of the samples by extrapolation the absorption edge onto the energy axis using Eq. 3 and that extracted from PL data.

Sample	Thickness (µm)	E_g (eV)	
		PL (a.u)	UV-Vis-NIR
Group I			
Sn_1	45.25	1.903	1.905
Sn_2	67.2	1.910	2.140
Sn_3	50.0	1.904	1.98
Group II			
Sp_1	13.0	1.902	1.805
Sp_2	33.5	1.905	2.080
Sp_3	16.0	1.903	1.920

From **Table 3** The values of E_g obtained for samples Sn_1, Sn_2 and Sn_3 are higher than Sp_1, Sp_2 and Sp_3, this due the increasing in layer thickness and light absorbing of PSL samples formed on front side lead to widening E_g of the materials **(Omar *et al.*, 2009).** Also, the average difference in band gap values that determined from PL and reflectance measurements is around 1.05% and 1.01% for PSL formed on front n and back p-side respectively.

4. Chemical composition of PSL (FTIR):

The FTIR spectra of the PS samples formed on front n and back p- side are display in **Fig. 8** and several spectral bands are presented in **Table 4.**

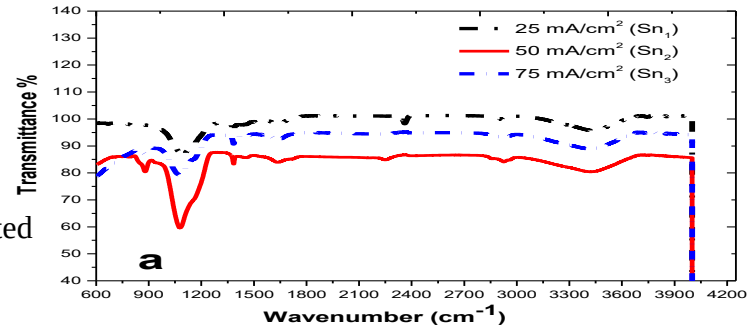

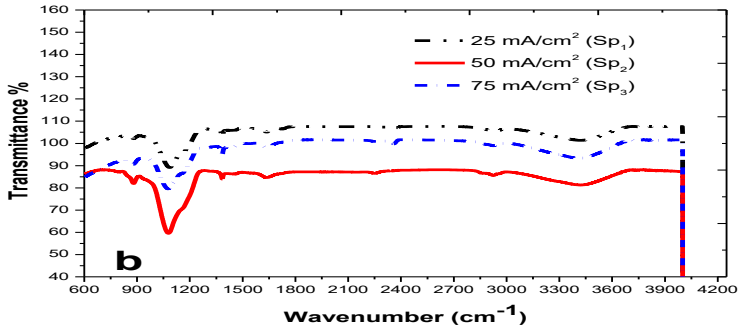

Figure 8. Transmittance of PSL samples prepared on (a): front n-side (Sn_1, Sn_2 and Sn_3**)** and (b): back p-side (Sp_1, Sp_2 and Sp_3).

Table 4. wavenumber position corresponding to the different surface species associated with the PSL surface.

Surface species	**Peak position (cm^{-1})**	**Modes**
O-H	3420.35	Strenching
C-H	2924.75	C-H_2 longitudinal asymmetric strenching
C-O	1640.00	Stretching vibration (bound group)
C-H3	1461.10	Asymmetric stretching
Si-O-Si	1078-1091	Si-O-Si Asymmetric stretching
Si-H_2	880.0	Si-o or Si-O-H bending
Si-H	630.0	Si-H bending

Comparing both FTIR and PL data, the following consistencies are produced.

(i) The FTIR spectra of the samples with a relatively high PL intensity exhibit a developed broad transmission bands for the two sample Sn_2 and Sp_2.

(ii) A supplementary distinguishing feature of the FTIR spectra of the samples that display high PL intensities is the existence of 2 major bonds are resulted: one around 856–891 cm^{-1} and the second around 3420 cm^{-1}. The last bonds are ascribed to O–H stretching modes. The band between 856 cm^{-1} and 895 cm^{-1} is related to oxygen complexes, mostly SiO stretching in O–SiO and

C–SiO, the formation of Si–O–Si bonds on the porous layers in the presence of humidity was detected by **Maruyama and Ohtani (1994),** Such presence of these bonds on the PSLs are responsible for the enhancement of PL intensity, and suggests that hydrogen passivation may not be the only parameter that responsible for the PL enhancement but depends on both hydrogen and oxygen passivation**.**

(iii) PL peak intensity and FTIR transmission peak intensity of PSL samples formed on front n-side are higher than those formed on the back p-side.

We can conclude that FTIR spectra of samples having higher bands concentrations attributed to hydrogen and oxygen complexes have more intense PL and lead to widen the band gap of the samples. So PSL is believed to be caused by a reduction in the Si dangling bond density. **(Lenshin *et al*., 2011)**.

5. Electrical properties of PSL:

The solar cells are fabricated after PSL formation on the surface of both front n-side **(group I samples)** and back p-side **(group II samples)** and both sides **(group III samples)** of n^+p/Si junction by ECE process

Few reports are reported on utilizing Au on PSL surface as front grid and Al for back surface contact by evaporation **(Zimin *et al*., 1995; Bhattacharya *et al*., 2000; Rabinal and Mulimani, 2005)**. These electrical contacts are used in order to measure J-V characteristics for the fabricated solar

cells. **Rabinal and Mulimani (2005)** denoted that Al can act electron injector as well (minority carrier device) while Au can act as improved hole injector (majority carrier device) so that, using these contacts are thoughted to be remarkable for refining solar cell conversion energy, and are suggested to increase surface stability of the solar cell.

Figure 9 represents the J–V characteristics of solar cells based on PSL formed on the front n-side (group I) and back p-side (group II) as well as cells without PSL have been measured at room temperature under dark and illumination of normal tungsten lamp with intensity of 100 mW/cm².

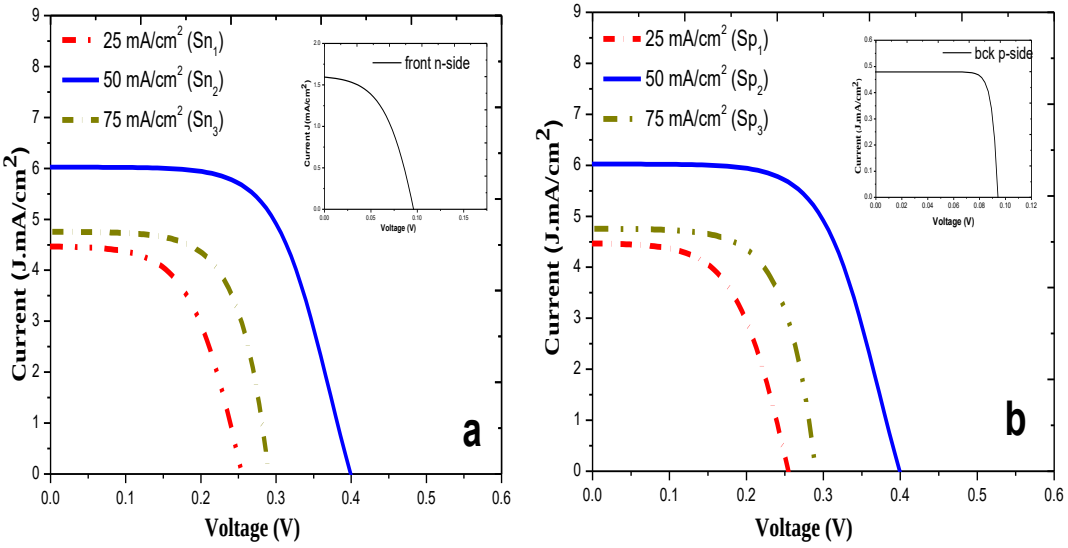

Figure 9. J-V characteristics of solar cell samples based on PSL prepared on (a): the front n-side (Sn_1, Sn_2, and Sn_3) and (b): back p-side (Sp_1, Sp_2 and Sp_3) under illumination of ordinary tungsten lamp of 100 mw/cm² compared with the solar cell without a PSL.

The open-circuit voltage (V_{oc}), short-circuit current (I_{sc}), maximum

Solar cell Samples	V max (V)	Jmax mA/cm²	Voc (V)	Isc (mA/cm²)	FF %	η %

voltage (V_m) and the maximum current (I_m) are the prominent parameters that are determined from measured J-V curve obtained, which used to investigate the efficiency (***η)*** of the solar cell **(Youssef *et al*., 2015a)**.

$$\eta = \frac{J_m V_m}{P_{in}} \text{……..(4)}$$

The degree of which V_m matches with V_{oc}, as well as the degree to which I_m matches with I_{sc} can be described by the fill factor (FF) **(Liu *et al*., 2014)**,

The fill factor (FF) was calculated by **Eq**. **5**

$$FF = \frac{P_m}{I_{SC} V_{OC}} = \frac{J_m V_m}{I_{SC} V_{OC}} \text{……..(5)}$$

GroupI						
front n-side (no PSL)	0.07	1.3	0.10	1.50	60.6	2.00
Sn1	0.24	3.0	0.28	3.25	79.00	2.25
Sn2	0.40	7.2	0.42	7.75	85.04	9.00
Sn3	0.30	4.5	0.35	4.80	80.35	4.20
GroupII						
Back p-side (no PSL)	0.08	0.40	0.10	0.70	45.70	1.00
Sp1	0.21	4.1	0.25	4.50	76.00	2.69
Sp2	0.35	5.7	0.4	6.00	81.10	6.23
Sp3	0.25	4.5	4.8	80.8	80.80	3.60

Table (5): different solar cells parameters based on the PSL prepared on the n-side and back p-side compared with the solar cell without a PSL.

The results above show that the two solar cells based on PSL formed on one side (front n and back p-side) at etching current of 50 mA/cm² give the best J-V characteristics. Thus, fabrication of solar cell based on both sides PSL at this condition would lead to increasing solar cell parameters, enhancing efficiency and reaching optimum condition for solar cell design that are best marketing in the industry.

Figure 10 characterizes J-V characteristics curves for solar cells samples based on both side PSL (group III) comparing to that based on one side PSL (group I and group II)

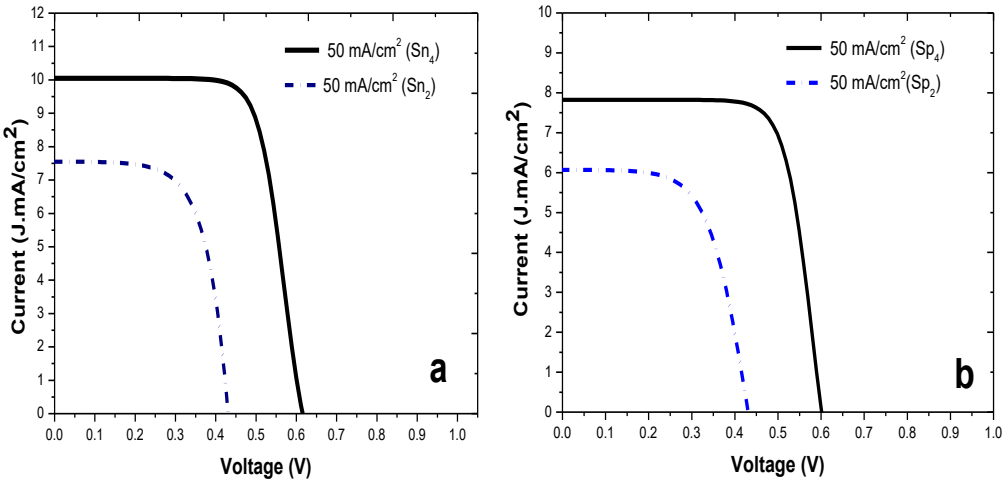

Figure 10. J-V characteristics of solar cell based on PSL prepared on (a): both sides (Sn_4 compared with that based one side ($Sn_{2)}$ and (b): both sides (Sp_4) compared with that based on one side (Sp_2).

Table 5. Different solar cells parameters based on the PSL prepared on both sides compared with that prepared on one side PSL at etching current density of 50 mA/cm^2.

Solar cell Samples	Group No.	V max (Vm)	Jmax (mA/cm^2)	Voc (V)	Isc (mA/cm^2)	FF%	η%
Sn_2	group I	0.40	7.2	0.42	7.75	85.04	9.0
Sn_4	group III	0.55	10.0	0.62	10.2	87.00	17.0
Sp_2	group II	0.35	5.7	0.40	6.0	81.10	6.23
Sp_4	group III	0.52	7.5	0.60	8.0	82.15	12.0

Table 5, shows that solar cell design based on both sides PSL provides stability and higher solar conversion efficiency solar cell conversion efficiency reach to 17.0% for sample Sn_4 with respect to other samples and it is be recommended for industry marketing.

CONCLUSION

In this work, PSL are fabricated on front, back and both sides of n^+-p/Si junctions by electrochemical etching for different current densities of 25, 50 and 75 mA/cm² and 25 etching time. SEM shows that pore diameter, porosity and thickness increase at current density of 50 mA/cm² for front and back side. The recorded PL intensities (broadening and height) and hence obtained Eg_s of PSL formed on front n-side are higher than that formed on the back p-side. The FTIR spectra of PSL samples having higher bands concentrations attributed to hydrogen and oxygen complexes have more intense PL and lead to widen the band gap of the samples. A reduction in light reflection of PSL samples by increasing in current density to 50 mA/cm² compared to un treated textured Si surface. The electrical parameters for solar cells based on both side PSL provides maximum solar conversion efficiency compared to solar cells based on side. So, we suggest that solar cell based on both side PSL provides stability and higher solar conversion efficiency of 17% and it is being recommended for industry marketing.

Acknowledgment

We would like to thank Prof. Dr. Halah Kassem, The Head of Basic Science Department, Institute of Environmental Studies and Research for providing many facilities, helpful discussion and kind encouragement during this work.

REFRENCES:

Anglin, E.J., Cheng, L., Freeman, W.R., and Sailor, M.J: (2006): Porous silicon in drug delivery devices and materials. *Advanced Drug Delivery Reviews*, 60, 1266-1255.

Bhattacharya, E., Ramesh, P., and Kumar, C.S. (2000): Studies on gold/porous silicon/crystalline silicon junctions. *Journal of Porous Materials*, 7, 299-301.

Bisi, O., Ossicini, S., & Pavesi, L. (2000): Porous silicon: a quantum sponge structure for silicon-based optoelectronics. *Surface science reports*, 36(1), 1-126.

Dian, J., Macek, A., Nižňanský, D., Němec, I., Vrkoslav, V., Chvojka, T., & Jelınek, I. (2004): SEM and HRTEM study of porous silicon relationship between fabrication, morphology and optical properties. *Applied Surface Science*, 236(1), 169-154.

Dzhafarov, T. (2013): Solar Cells-research and Application, Perspectives, in: A. Morales Acevedo (Ed.), Intech Open, USA.

Dubey, R. S., and Gautam, D. K. (2009): Fabrication and characterization of porous silicon layers for applications in optoelectronics. *Optical and Quantum Electronics*, 41(3), 169–201.

Fang, X., Rong, J., & Zhou, C. (2013): Review of porous silicon preparation and its application for lithium-ion battery anodes. *Nanotechnology*, 24(42), 422001.

Kulathuraan, K., Mohanraj, K., & Natarajan, B. (2016): Structural, optical and electrical characterization of nanostructured porous silicon: Effect of current density. *Spectrochimica Acta Part A: Molecular and Biomolecular Spectroscopy*, 152, 51-55.

Kubelka, P., & Munk, F. (1931): An article on optics of paint layers. *Technical Physics*, 12, 593-601.

Kubelka, P. (1946): New contributions to the optics of intensely light-scattering materials. Part I. *Josa*, 36(5), 446-455.

Len'shin, A. S., Kashkarov, V. M., Turishchev, S. Y., Smirnov, M. S., & Domashevskaya, E. P. (2011). Effect of natural aging on photoluminescence of porous silicon. *Technical Physics Letters*, 35(9), 569-592.

Liu, D., & Kelly, T. L. (2014): Perovskite solar cells with a planar heterojunction structure prepared using room-temperature solution processing techniques. *Nature photonics*, 6(2), 133-136.

Maruyama, T., Ohtani, S. (1994): Photoluminescence of porous silicon

exposed to ambient air. *Journal of Applied Physics Letter*, 65, 1346.

Omar, K., Hassan, Z., Ramzy, A., & Abu Hassan, H. (2009): Laser effects on porous silicon synthesis by photoelectrochemical etching process. *Journal of optoelectronics and advanced materials*, 11(11), 1641-1646.

Otsuka, M. (2004): Comparative particle size determination of phenacetin bulk powder by using Kubelka–Munk theory and principal component regression analysis based on near-infrared spectroscopy. *Powder Technology*, 141(3), 244-250.

Ou, W. Y., Zhang, Y., Li, H. L., Zhao, L., Zhou, C. L., Diao, H. W., & Wang, W. J. (2011). Effects of IPA on texturing process for mono-crystalline silicon solar cell in TMAH solution. *In Materials Science Forum*, 665, 31-35.

Rabinal, M.K. and Mulimani, B.G. (2005): Transport properties of molecularly stabilized porous silicon Schottky junctions. *New Journal of Physics*, 9, 440 -446.

Rajabi, M., & Dariani, R. S. (2009): Current improvement of porous silicon photovoltaic devices by using double layer porous silicon structure: applicable in porous silicon solar cells. *Journal of Porous Materials*, 16(5), 513-519.

Ramizy, A., Hassan, Z., Omar, K., Al-Douri, Y., & Mahdi, M. A. (2011): New optical features to enhance solar cell performance based on porous silicon surfaces. *Applied Surface Science*, 255(14), 6112-6115.

Salcedo, W. J., Ramirez Fernandez, F. J., & Galeazzo, E. (1995): Structural characterization of photoluminescent porous silicon with FTIR spectroscopy. *Brazilian Journal of Physics*, 25, 156-161.

Sailor, M.J. (2014): Fundamentals of Porous Silicon Preparation, Porous Silicon in Practice: Preparation, Characterization and Applications, *Wiley-VCH Verlag GmbH & Co. KGaA, Germany*, 1–42.

Salman, K. A., Hassan, Z., & Omar, K. (2012): Effect of silicon porosity on solar cell efficiency. *Intarnational Journal of Electrochemistry Scientific*, *5*(1), 356-366.

Salonen, J., Lehto, V. P., & Laine, E. (1995): The room temperature oxidation of porous silicon. *Applied surface science*, 120(3), 191-196.

Schneider B. W., Lal N. N., Baker-Finch S., White T. P. (2014): Pyramidal surface textures for light trapping and antireflection in perovskite-on-silicon tandem solar cells. *Optics Express*, 22(21), 1422-1430.

Singh P. K., Kumar R., Lal M., Singh S. N., Das B. K. (2001): Effectiveness of anisotropic etching of silicon in aqueous alkaline solutions. *Solar Energy Materials and Solar Cells*, 50(1):83–113.

Sun, K., Shen, S., Liang, Y., Burrows, P. E., Mao, S. S., & Wang, D. (2014): Enabling silicon for solar-fuel production. *Chemical reviews*, 114(15), 6662-6519.

Tauc, J., Grigorovici, R., & Vancu, A. (1966): Optical properties and electronic structure of amorphous germanium. *physica status solidi (b)*, 15(2), 625-635.

Uhlir, A. (1956): Electrolytic shaping of germanium and silicon. *Bell Labs Technical Journal*, 35(2), 333-345.

Yerokhov, V., Melnyk, I., Tsisaruk, A., & Semochko, I. (2000): Porous silicon in solar cell structures. *Optoelectronics Review*, (4), 414-415.

Youssef, G. M., El-Nahass, M. M., El-Zaiat, S. Y., & Farag, M. A. (2015a): Effect of porosity on the electrical and photoelectrical properties of textured n+ p silicon solar cells. *Materials Science in Semiconductor Processing*, 39, 455-466.

Youssef, G. M., El-Zaiat, S. Y., El-Malky, M., & Nawar, H. A. (2015b): preparation and physical characterization of porous silicon layers for sensing applications. *International Journal of Physics and Research (IJPR*), 5(3), 33-46.

Youssef, G. M. (2016): the effect of etching current on the formation of antireflection porous silicon coating fabricated by electrochemical technique for solar cells. *International Journal of Physics and Research (IJPR)*, 6(1), 5-20.

Zimin, S.P., Kuznetsov, V.S., and Prokaznikov, A.V. (1995): Electrical characteristics of aluminum contacts to porous silicon. *Applied Surface Scientific*, 91, 355–356.

تصنيع وتحسين خواص الخلية الشمسية السليكونية باستخدام طبقات السليكون المسامي على الجانبين الأمامي والخلفي للخلية

هاجر عبد الحكيم نوار [٣] ، جمال محمود يوسف[١]، محمود محمد النحاس[٢]، محمد غريب المالكي[٣]،

١) كلية العلوم – قسم الفيزياء – جامعة عين شمس
٢) كلية التربية– قسم الفيزياء– جامعة عين شمس
٣) معهد الدراسات والبحوث البيئية– قسم العلوم الأساسية البيئية – جامعة عين شمس

المستخلص

يعتبر السليكون المسامي ذو تطبيقات هامة في مجال الخلايا الشمسية وذلك بسب مساحة السطح الكبيرة نسبيا إلى الحجم، والتركيب الكيميائي السطحي الملائم. في هذه الدراسة تم تحضير عينات من طبقة السليكون المسامي من موصل سليكون من نوع (n^+p/Si) وذلك باستخدام عملية التنميش الكهروكيميائي عن طريق استخدام ثلاثة قيم مختلفة لكثافة التيار الكهربي ٢٥ ،٥٠، ٧٥ ملي أمبير/ سم^2. تم دراسة تأثير استخدام هذه القيم على الخواص السطحية (SEM) باستخدام الميكروسكوب الإلكتروني الماسح، الضوئية (PL) باستخدام مطياف الوميض الضوئي، الإنعكاسية (R) باستخدام مقياس الطيف الضوئي، الكيميائية (FTIR) باستخدام طيف الأشعة تحت الحمراء وخواص منحنى (J–V) باستخدام مصدر تيار كهربي من نوع (keithely 2400 source meter) لطبقات السليكون المسامي المحضر على الجانبين الأمامي والخلفي للموصل. أظهرت الخواص السطحية بالنسبة لطبقات السليكون المسامي على الجانب الأمامي للموصل عدم تماثل انتشار المسام على السطح كما أن المسام ذات احجام متفاوتة بمسامية في حدود٩٠ %. على النقيض فعينات السليكون المسامي المحضر على الجانب الخلفي يبدو فيها انتشار المسام على طول السطح بأحجام شبه متساوية ونسبة مسامية تصل إلى ٩٨% . يظهر طيف الوميض الضوئي لطبقة السليكون المسامي أعلى ارتفاع للقمه عند المدى الطيفي ٦٥٩ نانومتر وكثافة تيار بقيمة ٥٠ ملي أمبير/ سم^2 لكل من الجانبين الأمامي والخلفي للموصل. كما سجلت نتائج الإنعكاسية السطحية لطبقة السليكون المسامي المحضر على الوجهين الأمامي والخلفي للموصل أقل قيما لها لنفس كثافة التيار الكهربي. أوضح طيف الأشعة تحت الحمراء ظهور قمم ذات كثافة مرتفعة لنفس العينات ذات الكثافة العالية للوميض الطيفي. وقد حققت نتائج استخدام طبقة السليكون المسامي على الجانبين الأمامي والخلفي معا للخلية الشمسية إلى زيادة كفاءتها

بنسبة تصل إلى١٧ % لذلك فإن استخدام طبقات السليكون المسامي على الجانبين الأمامي والخلفي للخلية الشمسية يزيد من فاعليتها ويوصي به لإستخدامة كأحد المواد الهامة في صناعة الخلايا الشمسية.